

Article

Tuning of the PI Controller Parameters of a PMSG Wind Turbine to Improve Control Performance under Various Wind Speeds

Yun-Su Kim ^{1,*}, Il-Yop Chung ² and Seung-II Moon ¹

¹ School of Electrical and Computer Engineering, Seoul National University, Seoul 151-744, Korea; E-Mail: moonsi@plaza.snu.ac.kr

² School of Electrical Engineering, Kookmin University, Seoul 136-702, Korea; E-Mail: chung@kookmin.ac.kr

* Author to whom correspondence should be addressed; E-Mail: yskim@powerlab.snu.ac.kr; Tel.: +82-2-886-3101.

Academic Editor: Frede Blaabjerg

Received: 2 January 2015 / Accepted: 2 February 2015 / Published: 13 February 2015

Abstract: This paper presents a method to seek the PI controller parameters of a PMSG wind turbine to improve control performance. Since operating conditions vary with the wind speed, therefore the PI controller parameters should be determined as a function of the wind speed. Small-signal modeling of a PMSG WT is implemented to analyze the stability under various operating conditions and with eigenvalues obtained from the small-signal model of the PMSG WT, which are coordinated by adjusting the PI controller parameters. The parameters to be tuned are chosen by investigating participation factors of state variables, which simplifies the problem by reducing the number of parameters to be tuned. The process of adjusting these PI controller parameters is carried out using particle swarm optimization (PSO). To characterize the improvements in the control method due to the PSO method of tuning the PI controller parameters, the PMSG WT is modeled using the MATLAB/SimPowerSystems libraries with the obtained PI controller parameters.

Keywords: participation factor; permanent magnet synchronous generator wind turbine (PMSG WT); PI controller parameters; small-signal modeling

1. Introduction

The penetration of renewable energy resources has seen consistent growth in recent years [1,2]. In particular, the use of wind power has grown considerably, and as of the end of 2011 significant commercial installations have appeared in 80 countries, totaling approximately 240 GW; the average annual cumulative growth rate of wind power over the past 15 years has been approximately 28% [2,3]. Due to this increase in capacity, the specific technical requirements for wind turbines (WTs) have led to control issues [4].

In this paper we focus on improving the control of WTs by tuning the controller parameters depending on the wind speed. The wind speed is an important factor that determines the operating conditions of WTs, and may vary arbitrarily and in an unpredictable manner; controller parameters should therefore be tuned for various wind speeds. In this paper, the WTs considered are permanent magnet synchronous generator (PMSG) turbines. Along with doubly fed induction generator (DFIG) WTs [2,5], PMSGs are the most common type of WT; however, PMSG WTs are preferable, since the former have lower maintenance costs [2,6]. The maintenance cost is an important factor since most of the large-scale wind farms have been sited on off-shore recently. This phenomenon is due to its geographical limitation and environmental regulations for on-shore site. The controller is designed as a proportional-integral (PI) controller since it is the most common controller used in industrial applications today [7,8].

Many literatures on WT control performance issue have been published [4,9–15]. A comparison between a PMSG WT and a DFIG WT was studied from the stability perspective in [13], but no method for tuning controller parameters to improve control performance was proposed. In reference [4], two different PMSG WT control modes were compared with each other and analyzed from the power coefficient and stability perspectives. However, it did not contain any theoretical analysis such as small-signal analysis which gives more precise result of analysis. For precise analysis of the control performance, some early works have investigated using optimization algorithms and small-signal analysis. For instances, in reference [9], DFIG controller parameters were tuned by particle swarm optimization (PSO) and in reference [10], small-signal modeling and analysis was implemented and PI controller parameters were adjusted by investigating traces of eigenvalues. For other instances, a genetic algorithm (GA) was used in reference [11] to adjust the controller parameters of a PMSG WT and a torque compensation strategy for PMSG WTs to improve the system stability was presented in reference [12]. A major demerit of references [9–12], which is the main focus in the paper, is that they have only considered a fixed wind speed and that of references [10,12] is that they did not apply optimization algorithms, so they cannot guarantee that the designed controller parameters are optimized to their objective. A small-signal stability analysis of a DFIG WT was presented in references [14,15]. A controller parameter adjustment for different wind speeds was implemented in them, but the number of considered wind speed points for designing the controller parameters is insufficient to apply to various wind speeds. Overall, the small-signal modeling and analysis of a PMSG WT has been rarely researched [10].

In this paper, PI controller parameters of a PMSG WT for various wind speeds are designed to improve control performance. To this end, small-signal modeling is implemented for analyzing the control performance of a PMSG WT. Eigenvalues which can be obtained from a system matrix of the

small-signal model are coordinated by adjusting the PI controller parameters. The parameters to be tuned are selected by using participation factors to make the problem simple. The process of adjusting the parameters is conducted by using a PSO algorithm which uses the heuristic-based swarm intelligence concept. It is known to effectively solve large-scale nonlinear optimization problems and has fast convergence characteristics [16]. The effectiveness of the PI controller parameters obtained by the proposed method is verified by a simulation which applies them to a PMSG WT modeled in MATLAB/SimPowerSystems.

2. Small-Signal Modeling

Figure 1 shows the system to be analyzed, which contains a PMSG WT integrated with an infinite bus. It is composed of the WT drive train, a PMSG, a machine-side converter (MSC), a DC-link capacitor, a GSC, an RL-filter, and a transformer. In this section, each component of the system will be formulated into a state-space model, which will then be used to find the eigenvalues.

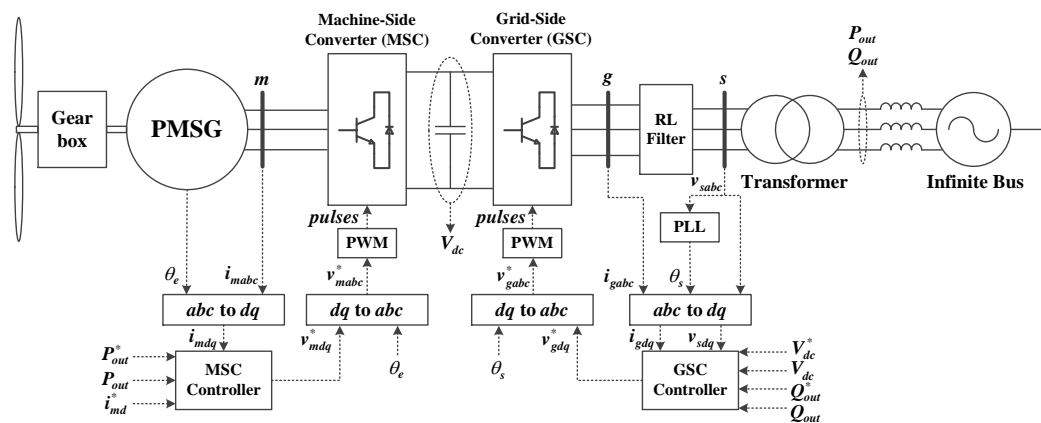


Figure 1. Schematic diagram of the system.

2.1. Wind Turbine Model

The power that can be extracted from the wind by a WT can be expressed as [17]:

$$P_w = \frac{1}{2} C_p(\lambda, \beta) \rho \pi r^2 v_w^3 \tag{1}$$

$$\lambda = \frac{\omega_t r}{v_w} \tag{2}$$

where λ is the tip-speed ratio, β is the pitch angle, ρ is the air density, r is the blade radius, v_w is the wind speed, ω_t is the rotational speed of the WT, and C_p is the power coefficient of WT which is a function of λ and β . C_p is given as [17]:

$$C_p = 0.73 \left(\frac{151}{\lambda_i} - 0.58\beta - 0.002\beta^{2.14} - 13.2 \right) e^{-18.4/\lambda_i} \tag{3}$$

$$\lambda_i = \left(\frac{1}{\lambda - 0.02\beta} + \frac{0.003}{\beta^3 + 1} \right)^{-1} \tag{4}$$

The pitch angle β is controlled only when v_w exceeds the rated wind speed to maintain the rated active power of the PMSG. Otherwise, it is kept constant at $\beta = 0^\circ$ which is the only considered value of β since only the operating conditions under the rated wind speed will be treated in this paper. Hence, it does not influence the small-signal modeling.

For a given v_w and β , there is an optimal rotational speed of the WT $\omega_{t,opt}$ which gives an optimal tip-speed ratio λ_{opt} [18,19]. It is essential to maintain $\omega_t = \omega_{t,opt}$ to maximize P_w which is an objective of the maximum power point tracking (MPPT) control. This means that it is to make C_p to the maximum value $C_{p,max}$, so the maximum power that can be extracted from the wind is given as [17]

$$P_{w,max} = K_{opt} \omega_{t,opt}^3 \quad (5)$$

$$K_{opt} = \frac{1}{2} C_{p,max} \rho \pi r^2 \left(\frac{r}{\lambda_{opt}} \right)^3 \quad (6)$$

It can be implemented by controlling the electrical rotational speed of the generator rotor ω_e , which has a following relationship with ω_t [17]:

$$\omega_e = N_{pp} \omega_m = N_{gr} N_{pp} \omega_t \quad (7)$$

where N_{pp} is the number of pole pairs in the PMSG, N_{gr} is the gear ratio, and ω_m is the mechanical rotational speed of the generator rotor. ω_m accelerates or decelerates respect to the WT driving torque equation [20]:

$$T_e - T_m = J_{eq} \frac{d\omega_m}{dt} \quad (8)$$

where T_e and T_m are the electromagnetic and the mechanical torque of the generator, respectively, and J_{eq} is the total equivalent inertia referred to the generator which contains the turbine and the generator inertia.

2.2. Permanent Magnet Synchronous Generator Model

Transforming a three-phase stator current i_{mabc} into the machine-side dq -reference frame aligned with the electrical rotor position θ_e , the voltage and torque equations of the salient-pole PMSG can be expressed as [20]:

$$v_{md} = R_s i_{md} + L_d \frac{di_{md}}{dt} - \omega_e L_q i_{mq} \quad (9)$$

$$v_{mq} = R_s i_{mq} + L_q \frac{di_{mq}}{dt} + \omega_e L_d i_{md} + \omega_e \lambda_{pm}$$

$$T_e = \frac{3}{2} N_{pp} \left\{ \lambda_{pm} i_{mq} + (L_d - L_q) i_{md} i_{mq} \right\} \quad (10)$$

where R_s is the stator resistance, λ_{pm} is the permanent magnetic flux, and v_{md} , v_{mq} , i_{md} , i_{mq} , L_d , and L_q are the d - and q -component of stator voltage, current, and inductance, respectively.

2.3. Machine-Side Converter Controller Model

The MSC control structure is shown in Figure 2. It consists of three PI controllers each of which controls the current i_{md} , i_{mq} , and the active power output P_{out} , respectively. Superscript * denotes the reference values of the PI controller inputs. From Equations (5)–(7), (9), we may determine expressions for the relevant MSC controller as follows:

$$\begin{aligned}
 i_{md}^* &= 0 \text{ A} \\
 R_s i_{md} + L_d \frac{di_{md}}{dt} &= K_{p1} (i_{md}^* - i_{md}) + K_{i1} \phi_1 \\
 \frac{d\phi_1}{dt} &= i_{md}^* - i_{md} \\
 P_{out}^* &= K_{opt} \left(\frac{\omega_e}{N_{pp} N_{gr}} \right)^3 \\
 P_{out} &= \frac{3}{2} (v_{sd} i_{sd} + v_{sq} i_{sq}) = \frac{3}{2} (v_{sd} i_{gd} + v_{sq} i_{gq}) = \frac{3}{2} v_{sd} i_{gd} \\
 i_{mq}^* &= K_{p2} (P_{out} - P_{out}^*) + K_{i2} \phi_2 \\
 \frac{d\phi_2}{dt} &= P_{out} - P_{out}^* \\
 R_s i_{mq} + L_q \frac{di_{mq}}{dt} &= K_{p3} (i_{mq}^* - i_{mq}) + K_{i3} \phi_3 \\
 \frac{d\phi_3}{dt} &= i_{mq}^* - i_{mq}
 \end{aligned} \tag{11}$$

where K_{p1} – K_{p3} and K_{i1} – K_{i3} are the p - and i -gains of the PI controllers, v_{sd} , v_{sq} , i_{sd} , and i_{sq} are the d - and q -axis voltage and current at the terminal of RL-filter, i_{gd} and i_{gq} are the GSC terminal d - and q -axis current, respectively, and ϕ_1 – ϕ_3 are the intermediate state variables introduced by the PI controllers. Imposing $i_{md}^* = 0$ is an optimal approach to avoid the nonlinearity of Equation (10) and to minimize current coupling [21,22]. This reduces Equation (10) to [23]:

$$T_e = \frac{3}{2} N_{pp} \lambda_{pm} i_{mq} \tag{12}$$

Regulating $i_{md}^* = 0$ guarantees minimum stator currents for a given torque, which enhances the mechanical efficiency [22]. When calculating P_{out} , since it passes through same current path, i_{sd} and i_{sq} can be set equal to i_{gd} and i_{gq} , respectively. Since the grid-side dq -reference frame is aligned with θ_s , which is the angular position of the RL-filter terminal voltage, $v_{sq} = 0$ which allows to eliminate v_{sq} term in P_{out} shown in Equation (11). The dynamic process of the converter can be ignored since it is much faster than electromagnetic and mechanical dynamic process, so it can be assumed that $v_{md}^* = v_{md}$, $v_{mq}^* = v_{mq}$ [10].

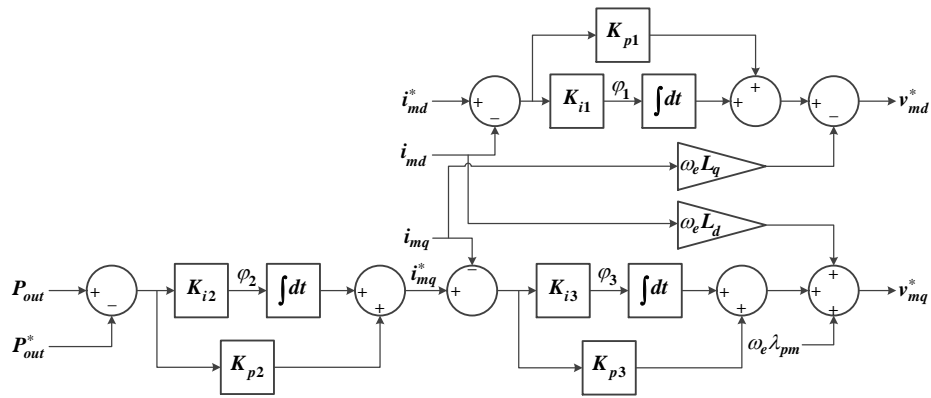


Figure 2. Control structure of MSC.

2.4. DC-Link Model

Figure 3 shows the power flow through the DC-link part from the PMSG to the power grid where C_{dc} is the capacitance of the DC-link capacitor, P_P and P_M are the active powers from the PMSG and the MSC, respectively, P_C , P_G , and P_F are the active powers flow into the DC-link capacitor, the GSC, and the RL-filter, respectively, and V_{dc} and I_{dc} are the DC-link voltage and current, respectively. Assuming that power losses in the MSC, the GSC, the RL-filter, and the transformer can be neglected, the active power transferred from the PMSG to the grid can be expressed as:

$$\begin{aligned}
 P_P &= \frac{3}{2}(-v_{md}i_{md} - v_{mq}i_{mq}) = P_M \\
 P_C &= V_{dc}I_{dc} = V_{dc}C_{dc} \frac{dV_{dc}}{dt} = P_M - P_G \\
 P_G &= P_F = P_{out}.
 \end{aligned}
 \tag{13}$$

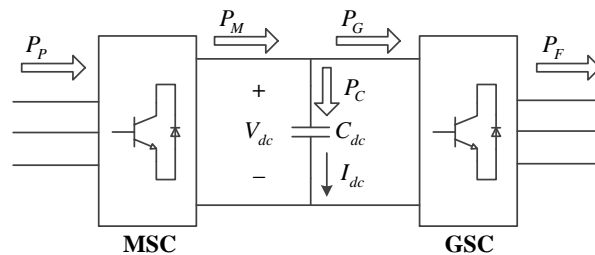


Figure 3. DC-link power flow.

2.5. Grid-Side Converter Controller Model

The voltage balance across the RL-filter shown in Figure 1 can be expressed as [20]:

$$\begin{aligned}
 v_{gd} &= R_f i_{gd} + L_f \frac{di_{gd}}{dt} - \omega_s L_f i_{gq} + v_{sd} \\
 v_{gq} &= R_f i_{gq} + L_f \frac{di_{gq}}{dt} + \omega_s L_f i_{gd} + v_{sq}
 \end{aligned}
 \tag{14}$$

where v_{gd} and v_{gq} are the GSC terminal d - and q -axis voltage, respectively, R_f and L_f are the resistance and the inductance of the RL-filter, respectively, and ω_s is the angular frequency of the RL-filter terminal voltage.

Figure 4 shows the structure of the GSC controller. It includes four PI controllers, which control V_{dc} , i_{gd} , i_{gq} , and the reactive power output Q_{out} , respectively. As that of the MSC controller, superscript * denotes for the reference values of the PI controller inputs. Based on Equation (14) and the control structure shown in Figure 4, the equations relevant to the GSC controller can be expressed as follows:

$$\begin{aligned}
 V_{dc}^* &= 5400 \text{ V} \\
 i_{gd}^* &= K_{p4}(V_{dc} - V_{dc}^*) + K_{i4}\phi_4 \\
 \frac{d\phi_4}{dt} &= V_{dc} - V_{dc}^* \\
 R_f i_{gd} + L_f \frac{di_{gd}}{dt} &= K_{p5}(i_{gd}^* - i_{gd}) + K_{i5}\phi_5 \\
 \frac{d\phi_5}{dt} &= i_{gd}^* - i_{gd} \\
 Q_{out}^* &= 0 \text{ VAR} \\
 Q_{out} &= \frac{3}{2}(v_{sq}i_{sd} - v_{sd}i_{sq}) = \frac{3}{2}(v_{sq}i_{gd} - v_{sd}i_{gq}) = -\frac{3}{2}v_{sd}i_{gq} \\
 i_{gq}^* &= K_{p6}(Q_{out} - Q_{out}^*) + K_{i6}\phi_6 \\
 \frac{d\phi_6}{dt} &= Q_{out} - Q_{out}^* \\
 R_f i_{gq} + L_f \frac{di_{gq}}{dt} &= K_{p7}(i_{gq}^* - i_{gq}) + K_{i7}\phi_7 \\
 \frac{d\phi_7}{dt} &= i_{gq}^* - i_{gq}
 \end{aligned}
 \tag{15}$$

where K_{p4} – K_{p7} and K_{i4} – K_{i7} are the p - and i -gains of the PI controllers, respectively, and ϕ_4 – ϕ_7 are the intermediate state variables introduced by the PI controllers. Imposing $Q_{out}^* = 0$ is to maintain the unity power factor. As mentioned in the previous section, i_{sd} and i_{sq} are equal to i_{gd} and i_{gq} , respectively, and $v_{qs} = 0$, so Q_{out} can be simplified as shown in Equation (15).

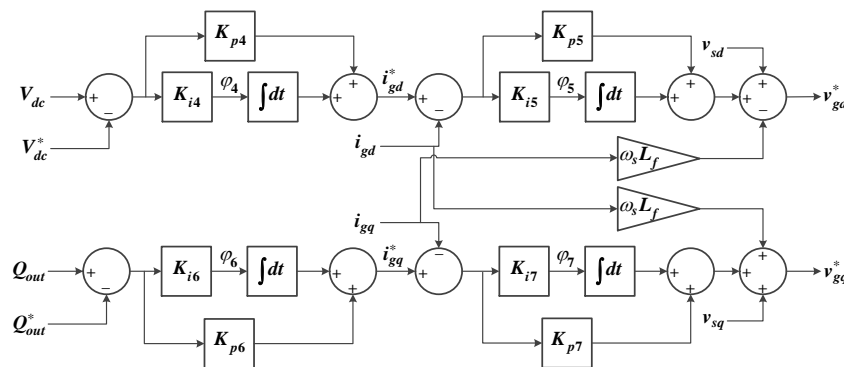


Figure 4. Control structure of GSC.

2.6. Power Grid Model

As shown in Figure 1, the PMSG WT is connected to the infinite bus via the transformer and the transmission line. To establish the equations of the power grid, assuming that the resistance of the transformer is neglected, the circuit on the right side of node *s* in Figure 1 can be simplified as Figure 5 where x_T and x_L are the reactances of the transformer and the transmission line, respectively, i_{gdq} is the GSC terminal *dq*-axis current, v_{sdq} is the RL-filter terminal *dq*-axis voltage, v_{idq} is the infinite bus *dq*-axis voltage, $|v_{sdq}|$ and $|v_{idq}|$ are the magnitude of v_{sdq} and v_{idq} , respectively, and δ is the angle of the infinite bus voltage relative to the reference angle. Since the reference angle is aligned to that of v_{sd} , the equation of the current flows into the power grid can be calculated as:

$$i_{gdq} = \frac{|v_{sdq}| \sin 0 - |v_{idq}| \sin \delta}{x_{TL}} + j \frac{-|v_{sdq}| \cos 0 + |v_{idq}| \cos \delta}{x_{TL}} \tag{16}$$

where x_{TL} is the summation of x_T and x_L . Since the power factor is maintained to unity, i_{gdq} is in phase with v_{sdq} . And this makes the real part and the imaginary part of i_{gdq} to be i_{gd} and i_{gq} , respectively. Thus i_{gd} and i_{gq} can be written as:

$$i_{gd} = -\frac{|v_{idq}| \sin \delta}{x_{TL}}$$

$$i_{gq} = \frac{-v_{sd} + |v_{idq}| \cos \delta}{x_{TL}} \tag{17}$$

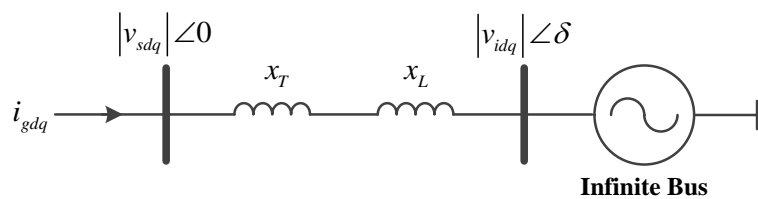


Figure 5. One-line diagram of the power grid.

2.7. Complete Small-Signal Model

To analyze the system stability following a change in the wind speed, and to evaluate the effectiveness of the controller parameters for the whole system, it is necessary to establish a complete small-signal model of the PMSG WT. By linearizing Equations (1)–(17), small-signal state-space equations of the PMSG WT can be obtained as follows:

$$\dot{x} = Ax + Bu$$

$$y = Cx + Du$$

$$x = [\omega_e \ i_{md} \ i_{mq} \ V_{dc} \ i_{gd} \ i_{gq} \ \varphi_1 \ \varphi_2 \ \varphi_3 \ \varphi_4 \ \varphi_5 \ \varphi_6 \ \varphi_7]^T \tag{18}$$

$$u = [v_w \ i_{md}^* \ V_{dc}^* \ Q_{out}^*]^T$$

$$y = [P_{out} \ Q_{out}]^T$$

where the individual elements of matrix A , which are derived as explained in the Appendix, are given at the bottom of the page and the subscript 0 appears in the elements of A denotes for the initial value. The matrices B , C , and D are unnecessary to calculate since the main purpose of the small-signal modeling is to acquire eigenvalues of A . It is sufficient to analyze the system stability only with the eigenvalues of A since they are identical to the system poles before cancellation of common poles and zeroes in the transfer function [24].

$$A = \begin{bmatrix} a_{1,1} & a_{1,2} & a_{1,3} & 0 & 0 & 0 & 0 & 0 & 0 & 0 & 0 & 0 & 0 \\ 0 & a_{2,2} & 0 & 0 & 0 & 0 & a_{2,7} & 0 & 0 & 0 & 0 & 0 & 0 \\ a_{3,1} & 0 & a_{3,3} & 0 & a_{3,5} & a_{3,6} & 0 & a_{3,8} & a_{3,9} & 0 & 0 & 0 & 0 \\ a_{4,1} & a_{4,2} & a_{4,3} & a_{4,4} & a_{4,5} & a_{4,6} & a_{4,7} & a_{4,8} & a_{4,9} & 0 & 0 & 0 & 0 \\ 0 & 0 & 0 & a_{5,4} & a_{5,5} & 0 & 0 & 0 & 0 & a_{5,10} & a_{5,11} & 0 & 0 \\ 0 & 0 & 0 & 0 & a_{6,5} & a_{6,6} & 0 & 0 & 0 & 0 & 0 & a_{6,12} & a_{6,13} \\ 0 & a_{7,2} & 0 & 0 & 0 & 0 & 0 & 0 & 0 & 0 & 0 & 0 & 0 \\ a_{8,1} & 0 & 0 & 0 & a_{8,5} & a_{8,6} & 0 & 0 & 0 & 0 & 0 & 0 & 0 \\ a_{9,1} & 0 & a_{9,3} & 0 & a_{9,5} & a_{9,6} & 0 & a_{9,8} & 0 & 0 & 0 & 0 & 0 \\ 0 & 0 & 0 & a_{10,4} & 0 & 0 & 0 & 0 & 0 & 0 & 0 & 0 & 0 \\ 0 & 0 & 0 & a_{11,4} & a_{1,5} & 0 & 0 & 0 & 0 & a_{11,10} & 0 & 0 & 0 \\ 0 & 0 & 0 & 0 & a_{12,5} & a_{12,6} & 0 & 0 & 0 & 0 & 0 & 0 & 0 \\ 0 & 0 & 0 & 0 & a_{13,5} & a_{13,6} & 0 & 0 & 0 & 0 & 0 & a_{13,12} & 0 \end{bmatrix}$$

$$a_{1,1} = \frac{9.305 \rho \pi r^2 v_{w0}^3 N_{pp}^2}{2J_{eq} \omega_{e0}^2} \left(\frac{217.965 v_{w0}^2 N_{pp}^2 N_{gr}^2}{r^2 \omega_{e0}^2} - \frac{42.092 v_{w0} N_{pp} N_{gr}}{r \omega_{e0}} + 1 \right) \exp \left(\frac{-18.4 v_{w0} N_{pp} N_{gr}}{r \omega_{e0}} - 0.0552 \right), \quad a_{1,2} = \frac{3N_{pp}^2}{2J_{eq}} (L_d - L_q) i_{mq0},$$

$$a_{1,3} = \frac{3N_{pp}^2}{2J_{eq}} \left\{ \lambda_{pm} + (L_d - L_q) i_{md0} \right\}, \quad a_{2,2} = \frac{-K_{p1} - R_s}{L_d}, \quad a_{2,7} = \frac{K_{i1}}{L_d}, \quad a_{3,1} = \frac{-3K_{opt} K_{p2} K_{p3} \omega_{e0}^2}{L_q N_{pp}^3 N_{gr}^3}, \quad a_{3,3} = \frac{-K_{p3} - R_s}{L_q}, \quad a_{3,5} = \frac{3K_{p2} K_{p3}}{2L_q} \left(v_{sd0} - \frac{x_{TL}^2 i_{gd0}^2}{v_{sd0} + x_{TL} i_{gq0}} \right),$$

$$a_{3,6} = \frac{-3K_{p2} K_{p3} x_{TL} i_{gd0}}{2L_q}, \quad a_{3,8} = \frac{K_{i2} K_{p3}}{L_q}, \quad a_{3,9} = \frac{K_{i3}}{L_q}, \quad a_{4,1} = \frac{3i_{mq0}}{2C_{dc} V_{dc0}} \left\{ i_{md0} L_q - \left(\frac{3K_{opt} K_{p2} K_{p3} \omega_{e0}^2}{N_{pp}^3 N_{gr}^3} + L_d i_{md0} + \lambda_{pm} \right) \right\}, \quad a_{4,2} = \frac{3}{2C_{dc} V_{dc0}} (K_{p1} i_{md0} - v_{md0} - \omega_{e0} L_d i_{mq0}),$$

$$a_{4,3} = \frac{3}{2C_{dc} V_{dc0}} (\omega_{e0} L_q i_{md0} - v_{mq0} + K_{p3} i_{mq0}), \quad a_{4,4} = \frac{3(v_{md0} i_{md0} + v_{mq0} i_{mq0} + v_{sd0} i_{gd0})}{2C_{dc} V_{dc0}^2}, \quad a_{4,5} = \frac{3}{2C_{dc} V_{dc0}} \left\{ \frac{3K_{p2} K_{p3} i_{mq0}}{2} \left(\frac{x_{TL}^2 i_{gd0}^2}{v_{sd0} + x_{TL} i_{gq0}} - v_{sd0} \right) - v_{sd0} + \frac{x_{TL}^2 i_{gd0}^2}{v_{sd0} + x_{TL} i_{gq0}} \right\},$$

$$a_{4,6} = \frac{3x_{TL} i_{gd0}}{2C_{dc} V_{dc0}} \left(1 - \frac{3K_{p2} K_{p3} i_{mq0}}{2} \right), \quad a_{4,7} = \frac{-3K_{i1} i_{md0}}{2C_{dc} V_{dc0}}, \quad a_{4,8} = \frac{-3K_{i2} K_{p3} i_{mq0}}{2C_{dc} V_{dc0}}, \quad a_{4,9} = \frac{-3K_{i3} i_{mq0}}{2C_{dc} V_{dc0}}, \quad a_{5,4} = \frac{K_{p4} K_{p5}}{L_f}, \quad a_{5,5} = \frac{-K_{p5} - R_f}{L_f}, \quad a_{5,10} = \frac{K_{i4} K_{p5}}{L_f}, \quad a_{5,11} = \frac{K_{i5}}{L_f},$$

$$a_{6,5} = \frac{3K_{p6} K_{p7} x_{TL}^2 i_{gd0} i_{gq0}}{2L_f (v_{sd0} + x_{TL} i_{gq0})}, \quad a_{6,6} = \frac{1.5K_{p6} K_{p7} (x_{TL} i_{gq0} - v_{sd0}) - R_f - K_{p7}}{L_f}, \quad a_{6,12} = \frac{K_{i6} K_{p7}}{L_f}, \quad a_{6,13} = \frac{K_{i7}}{L_f}, \quad a_{7,2} = -1, \quad a_{8,1} = \frac{-3K_{opt} \omega_{e0}^2}{N_{pp}^3 N_{gr}^3}, \quad a_{8,5} = \frac{3}{2} \left(v_{sd0} - \frac{x_{TL}^2 i_{gd0}^2}{v_{sd0} + x_{TL} i_{gq0}} \right),$$

$$a_{8,6} = \frac{-3x_{TL} i_{gd0}}{2}, \quad a_{9,1} = \frac{-3K_{opt} K_{p2} \omega_{e0}^2}{N_{pp}^3 N_{gr}^3}, \quad a_{9,3} = -1, \quad a_{9,5} = \frac{3K_{p2}}{2} \left(v_{sd0} - \frac{x_{TL}^2 i_{gd0}^2}{v_{sd0} + x_{TL} i_{gq0}} \right), \quad a_{9,6} = \frac{-3K_{p2} x_{TL} i_{gd0}}{2}, \quad a_{9,8} = K_{i2}, \quad a_{10,4} = 1, \quad a_{11,4} = K_{p4}, \quad a_{11,5} = -1,$$

$$a_{11,10} = K_{i4}, \quad a_{12,5} = \frac{3x_{TL}^2 i_{gd0} i_{gq0}}{2(v_{sd0} + x_{TL} i_{gq0})}, \quad a_{12,6} = \frac{3(x_{TL} i_{gq0} - v_{sd0})}{2}, \quad a_{13,5} = \frac{3K_{p6} x_{TL}^2 i_{gd0} i_{gq0}}{2(v_{sd0} + x_{TL} i_{gq0})}, \quad a_{13,6} = \frac{3K_{p6} (x_{TL} i_{gq0} - v_{sd0})}{2} - 1, \quad a_{13,12} = K_{i6}.$$

3. Optimization Algorithm

Here PSO is employed due to the effectiveness in solving optimization problems. A brief introduction to the PSO algorithm follows, together with the problem formulation.

3.1. Particle Swarm Optimization Algorithm

PSO is part of the swarm intelligence family of algorithms, which are known to effectively solve large-scale nonlinear optimization problems [16]. It exhibits excellent performance in searching for the global optimum because it can diversify the swarm using a stochastic velocity term [25]. Particles look for the optimal solution in search space based on position, which is learnt heuristically and iteratively. The movement of the particles is based on the following relations [25]:

$$V_i^{k+1} = wV_i^k + c_1 rand_1 (X_{lb,i}^k - X_i^k) + c_2 rand_2 (X_{gb}^k - X_i^k) \quad (19)$$

$$X_i^{k+1} = X_i^k + V_i^{k+1} \quad (20)$$

$$w = w_{max} - \frac{k(w_{max} - w_{min})}{N} \quad (21)$$

where X is the position vector, V is the velocity vector, w is the inertia weight, I is the particle index, k is the iteration index, X_{lb} and X_{gb} are the local and global optimum positions of the swarm, and N is the total number of iterations. The parameters c_1 and c_2 are the two acceleration constants, and $rand_1$ and $rand_2$ are two random numbers with a uniform distribution in the range [0.0, 1.0]. Typically, the maximum value of $c_1 + c_2$ should be 4.0, and an effective initial condition is $c_1 = c_2 = 2$ [16,26,27]. In this paper, c_1 , c_2 , w_{max} , and w_{min} are set to 2, 2, 1, and 0.1, respectively, grounds for experimental results.

3.2. Problem Formulation

The goal of the optimization algorithm is to minimize the objective function J which is given as:

$$J = \frac{1}{\left| \max_{j=1,2,\dots,13} \{ \text{Re}(\lambda_j) \} \right|} + f_p \quad (22)$$

$$f_p = \begin{cases} 1000, & \text{if } \max_{j=1,2,\dots,13} \{ \text{Re}(\lambda_j) \} \geq 0 \\ 0, & \text{otherwise} \end{cases}$$

where λ_j is the j th mode eigenvalue of the system matrix A in Equation (18) and f_p is the penalty function which is for determining whether the system is stable or not. Equation (22) is referred to in reference [25] with a slight modification of the penalty function. If the system is unstable or marginally stable which means the maximum value of the real part of eigenvalues is larger than or equal to 0, f_p becomes larger to prevent unstable or marginally stable system. The minimum and the maximum values for p - and i -gains of the PI controllers are set to 0.01 p.u. and 20 p.u., respectively. The PI controller parameters will be set to the minimum if they are lesser than the minimum and will be set to the maximum if they are larger than the maximum.

4. Case Studies

Three cases are studied in this paper to investigate the effectiveness of the proposed method. In Case I, the PI controller parameters, which are obtained by an experimental simulation test, are used to test the control performance of the PMSG WT. A classical method of tuning the parameters is adopted in Case II. In this case, participation factors of state variables of Case I are acquired, and then the PI controller parameters to be tuned are chosen. With changing the selected parameters, traces of eigenvalues are obtained. By observing the trace of eigenvalues, parameters that place eigenvalue at the leftmost point of the complex plane can be selected. The last case is the proposed method which uses PSO to minimize the objective function J in Equation (22). This optimization algorithm is applied to various wind speed points to change the parameters if the wind speed is changed. At every wind speed, participation factors are obtained to select the PI controller parameters to be controlled.

4.1. Case I—Adjusting Experimentally

In Case I, the PI controller parameters are adjusted heuristically by simulation test. This was done by MATLAB/SimPowerSystems model of the test system. After the test model is established, PI controller parameters are acquired by running simulation with trial and error. Among a number of trial runs of simulation by changing the parameters, a set of them that gives the best simulation results are chosen. They are shown in Table 1. With these parameters, the eigenvalues are obtained at the wind speed of 8 m/s and they are shown in Table 2. As shown in Table 2 for Case I, all of the real parts of the eigenvalues are negative, so the system is stable. However, to improve control performance, it is essential to move the dominant system poles, which are the eigenvalues that have large value of real part relative to the others, to the left side of the complex plane. In this case, λ_5 and λ_6 are of interest to relocate. The classical method to carry out this procedure is investigated in Case II.

Table 1. PI controller parameters for three cases at $v_{w0} = 8$ m/s.

Parameters	Value (in p.u.)		
	Case I	Case II	Proposed method
K_{p1}	1	1	4.14
K_{i1}	1	1	4.10
K_{p2}	0.1	0.01	0.01
K_{i2}	0.01	0.06	0.14
K_{p3}	1	1	0.73
K_{i3}	0.2	0.2	2.57
K_{p4}	1	1	2.91
K_{i4}	0.5	0.5	3.78
K_{p5}	1	1	17.46
K_{i5}	0.2	0.2	17.15
K_{p6}	1	1	4.61
K_{i6}	1	1	3.82
K_{p7}	1	1	2.12
K_{i7}	1.2	1.2	0.21

Table 2. Eigenvalues for three cases at $v_{w0} = 8$ m/s.

Index	Eigenvalues		
	Case I	Case II	Proposed method
λ_1	-720.76	-713.70	-13945.12
λ_2	-333.29	-341.44	-165.88 + j627.30
λ_3	-13.98 + j80.97	-7.67 + j78.26	-25.21 + j202.28
λ_4	-13.98 - j80.97	-7.67 - j78.26	-25.21 - j202.28
λ_5	-2.36 + j80.59	-7.01 + j6.53	-15.01
λ_6	-2.36 - j80.59	-7.01 - j6.53	-15.03
λ_7	-80.56	-80.32	-379.52
λ_8	-95.76	-98.24	-165.88 - j627.30
λ_9	-261.31 + j357.16	-261.31 + j357.16	-1673.04
λ_{10}	-261.31 - j357.16	-261.31 - j357.16	-480.39
λ_{11}	-737.57 + j503.99	-737.57 + j503.99	-9524.57
λ_{12}	-737.57 - j503.99	-737.57 - j503.99	-37.22
λ_{13}	-176.62	-176.62	-264.98

4.2. Case II—Classical Method

Since there were 14 PI controller parameters in the PMSG WT system, selecting parameters that are strongly related to the dominant poles is helpful to make the problem simpler. This procedure can be carried out by searching the relationship between the eigenvalues and the state variables from participation factors of those state variables [28,29].

Table 3 lists the participation factors. It can be seen that the eigenvalues to be relocated are dependent on the two state variables ω_e and φ_2 , which are related to the parameters K_{p2} and K_{i2} , as can be seen from Figure 2. To coordinate dominant system poles at the leftmost point of the complex plane, the traces of the dominant system poles K_{p2} and K_{i2} are plotted, as shown in Figure 6. Here λ_5 moves to the left-hand side of the complex plane, whereas λ_6 moves to the right-hand side and, eventually, the real part of it becomes larger than 0, which indicates that the system became unstable.

Table 3. Magnitudes of participation factors of state variables for Case I.

	λ_1	λ_2	$\lambda_{3,4}$	$\lambda_{5,6}$	λ_7	λ_8	$\lambda_{9,10}$	$\lambda_{11,12}$	λ_{13}
ω_e	0	0	0	0.51	0	0	0	0	0
i_{md}	0	0	0	0	0	0	0.62	0	0
i_{mq}	0.01	1.38	0.01	0	0	0.39	0	0	0
V_{dc}	0.03	0.01	0.54	0	0.03	0	0	0	0
i_{gd}	1.14	0.02	0.05	0	0.08	0	0	0	0
i_{gq}	0	0	0	0	0	0	0	1.05	0.05
φ_1	0	0	0	0	0	0	0.62	0	0
φ_2	0	0	0.01	0.52	0	0	0	0	0
φ_3	0	0.4	0	0	0.01	1.41	0	0	0
φ_4	0.01	0.02	0.53	0	0.05	0.01	0	0	0
φ_5	0.13	0	0.03	0	1.17	0.02	0	0	0
φ_6	0	0	0	0	0	0	0	0.27	0.86
φ_7	0	0	0	0	0	0	0	0.82	0.09

Figure 6b illustrates that λ_5 and λ_6 initially move toward the left-hand side of the complex plane, until the real part becomes approximately -15 ; subsequently one of them moves in the opposite direction and the other continues to move in the same direction. The traces of λ_3 and λ_4 should be noted, since they move to the right-hand side as K_{i2} increases. From the traces of eigenvalues, we may conclude that K_{p2} should be decreased and K_{i2} should be increased appropriately. Tuned values of the parameters and the corresponding eigenvalues for Case II are listed in Tables 1 and 2, respectively. It can be seen that the real parts of λ_5 and λ_6 in Case II were smaller than in Case I; however, the real parts of λ_3 and λ_4 became larger and approached those of λ_5 and λ_6 . In this case, other parameters that those related to λ_3 and λ_4 should also be adjusted to improve the control system; however, it is not straightforward to search the traces of eigenvalues. To solve this problem, we apply PSO, as described in the following subsection.

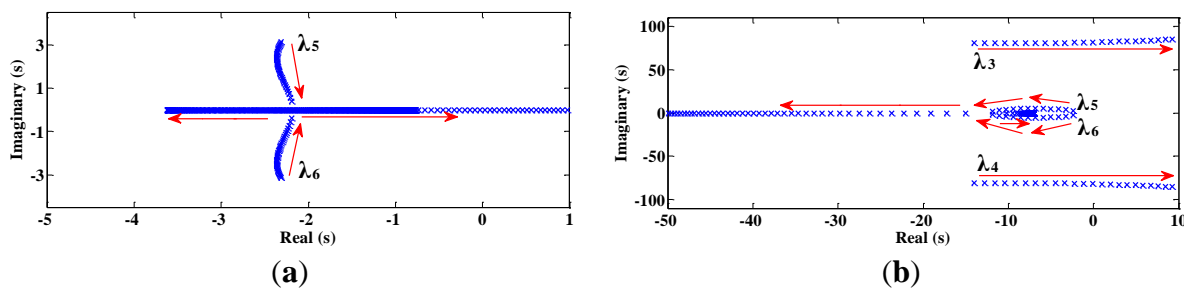


Figure 6. Eigenvalue analysis. (a) Trace of the dominant poles when K_{p2} increases; (b) Trace of the dominant poles when K_{i2} increases.

4.3. Case III—Proposed Method

Figure 7 shows a flow chart of the PSO method. At wind speed intervals of 0.1 m/s from the cut-in wind speed of 3 m/s to the rated wind speed 11 m/s, the PI controller parameters that minimize J were searched for. Initially, the wind speed was set to $v_w = 3$ m/s and all of the parameters were adjusted to minimize J . Then v_w was increased by 0.1 m/s, with the optimized parameters acquired using PSO at $v_w = 3$ m/s used to initialize the problem. The dominant pole p_d was determined, which had the largest real part, and the other poles with real parts that were of similar magnitude to that of p_d (with a difference of less than a tolerance ϵ) were found, if they existed. This tolerance for locating additional significant pole was $\epsilon = 0.5$. A set of PI controller parameters S_p , which are strongly dependent on the dominant poles, were searched for by using the participation factors. By setting these parameters S_p as variables to be tuned, rather than all 14 parameters, the minimization of J is simplified. The PSO algorithm was then implemented to obtain the parameter set S_p . This process was repeated in 0.1-m/s increments of v_w , up to $v_w = 11$ m/s.

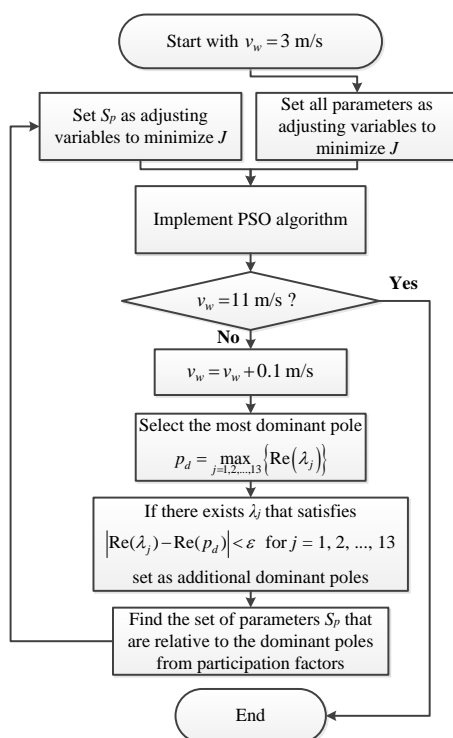


Figure 7. The whole flow chart of the proposed method.

The resulting PI controller parameters are shown in Figure 8, where K_{p2} , K_{i2} , K_{p4} , and K_{i4} are plotted as a function of the wind speeds in the range $3 \leq v_w \leq 11$ m/s. The other parameters remained the same as those listed in Table 1, which were obtained at $v_w = 3$ m/s. As shown in Table 4, the dominant poles at $v_w = 3$ m/s were λ_5 and λ_6 and were strongly dependent on the state variables ω_e and φ_2 , which follows from the participation factors. Those variables are related to K_{p2} and K_{i2} , as mentioned previously, which is to be expected since they are the controller parameters that determine the active power, and react much more slowly than those that determine the currents. During the PSO optimization, K_{p2} remained constant at the minimum, since it tended to decrease for the whole range of the wind speeds. The parameter K_{i2} also tended to decrease as the wind speed increased. Only these two parameters were controlled until the real part value of λ_3 and λ_4 became closer to those of λ_5 and λ_6 at $v_w = 9.9$ m/s (see Table 4). Thus at $v_w = 10$ m/s, K_{p4} and K_{i4} (which are related to λ_3 and λ_4) were also selected as parameters to be modified. After adjusting K_{p4} and K_{i4} at $v_w = 10$ m/s, the real parts of λ_5 and λ_6 became much smaller than those of λ_3 and λ_4 (see Table 4). Subsequently, only K_{p2} and K_{i2} were adjusted for wind speeds of $v_w > 10$ m/s.

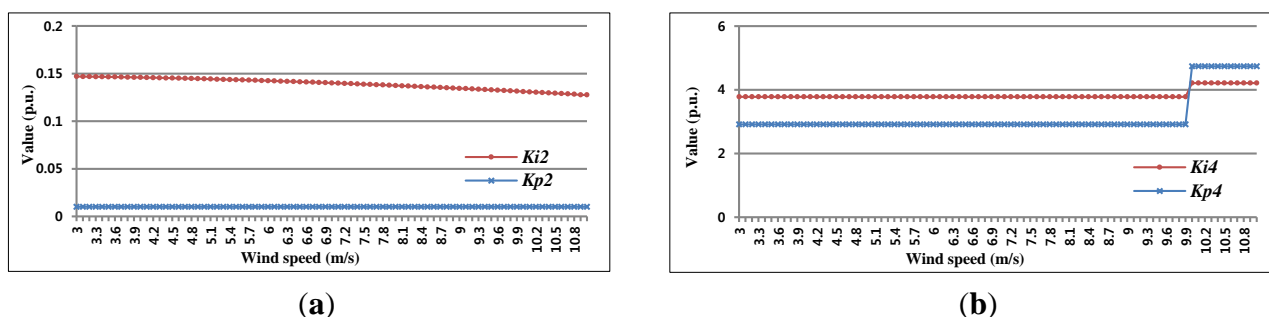


Figure 8. The parameters obtained by using PSO algorithm for various wind speeds. (a) K_{p2} and K_{i2} for $v_w = 3$ –11 m/s. (b) K_{p4} and K_{i4} for $v_w = 3$ –11 m/s.

Table 4. Eigenvalues for the proposed method at particular wind speeds.

Index	Eigenvalues		
	$v_w = 3$ m/s	$v_w = 9.9$ m/s	$v_w = 10$ m/s
λ_1	-13944.43	-13946.34	-13888.08
λ_2	-160.40 + j626.99	-168.52 + j627.74	-173.50 + j623.71
λ_3	-39.60 + j208.09	-18.75 + j197.66	-42.21 + j205.74
λ_4	-39.60 - j208.09	-18.75 - j197.66	-42.21 - j205.74
λ_5	-5.68 + j0.002	-18.45	-18.65 + j0.006
λ_6	-5.68 - j0.002	-18.47	-18.65 - j0.006
λ_7	-379.47	-379.55	-380.57
λ_8	-160.40 - j626.99	-168.52 - j627.74	-173.50 - j623.71
λ_9	-1673.04	-1673.04	-1673.04
λ_{10}	-480.39	-480.39	-480.39
λ_{11}	-9524.57	-9524.57	-9524.57
λ_{12}	-37.22	-37.22	-37.22
λ_{13}	-264.98	-264.98	-264.98

5. Simulation Verification

The effectiveness of the proposed method was investigated using simulations. The parameters listed in Table 1 were applied to the PMSG WT modeled using the MATLAB/SimPowerSystems libraries. The parameters describing the PMSG WT system are given in the Appendix. Due to the large number of sets of PI controller parameters for the whole range of wind speeds considered in Case III, we describe a simulation test at $v_w = 8$ m/s, since this can demonstrate the superiority of the PSO method.

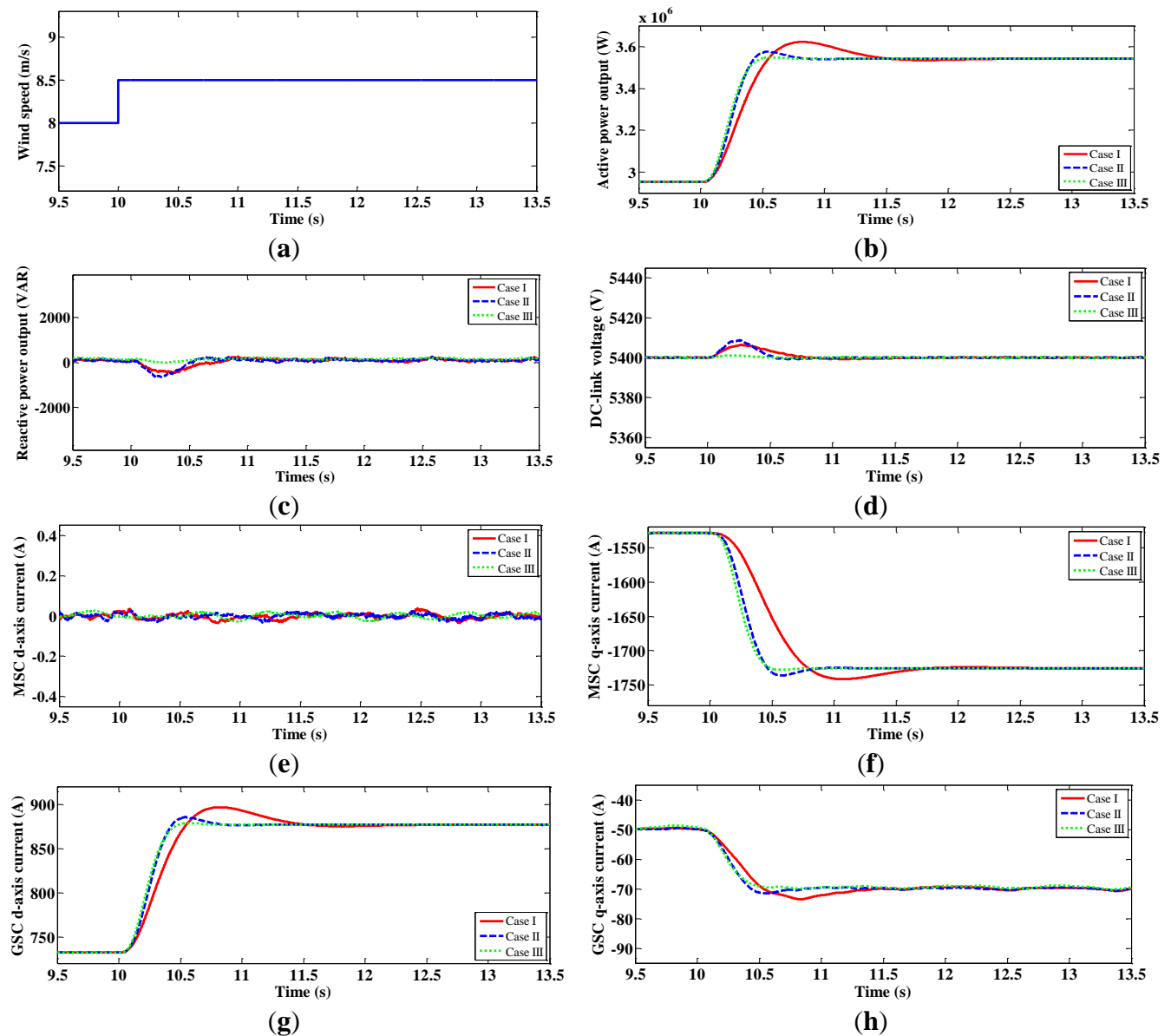


Figure 9. Simulation test results for three cases. (a) Wind speed; (b) Active power output; (c) Reactive power output; (d) DC-link voltage; (e) MSC *d*-axis current; (f) MSC *q*-axis current; (g) GSC *d*-axis current; (h) GSC *q*-axis current.

Figure 9a shows the time dependence of the wind speed that was applied to the PMSG WT, and Figure 9b–h show the dynamics of the system state variables and output variables for the three control methods. The data were filtered using a low-pass filter to provide a better comparison, as the original signals contained harmonic distortion. From Figure 9b,f–h, it can be seen that the signals from the PSO

method (Case III) stabilized the system to a steady-state more rapidly than those of the other control methods. Moreover, overshoots of the signals were smaller with the PSO method. From Figure 9c,d, we can see improved performance in terms of Q_{out} and V_{dc} with the PSO method, which maintained their reference values well, whereas those of the other methods temporarily deviated from the reference values.

6. Conclusions

We have described a tuning method for the PI controller parameters of a PMSG WT. To acquire the dominant poles of the system and evaluate the stability, a small-signal analysis of the PMSG WT was carried out. The PI controller parameters were then adjusted to minimize the real part of the dominant poles. This process was implemented using a PSO algorithm, which is an efficient algorithm to solve nonlinear optimization problems.

Since the operating conditions of the PMSG WT change when the wind speed fluctuates, parameter sets were obtained for the wind speeds with 0.1 m/s increments in the range from the cut-in speed to the rated speed (*i.e.*, 3–11 m/s). To simplify the problem, the PI controller parameters that were strongly related to the dominant poles were selected to be adjusted using the PSO algorithm using the participation factors; this was carried out for each wind speed investigated, except $v_w = 3$ m/s, for which all parameters were optimized.

To verify the effectiveness of the proposed method, the PMSG WT shown in Figure 1 was modeled using the MATLAB/SimPowerSystems libraries. Based on these simulated data, we may conclude that the control performance of the proposed method gives faster rising and settling time and has smaller overshoot than those of the other cases.

Acknowledgments

This work was supported by the Human Resources Development program (No. 20124030200030) of the Korea Institute of Energy Technology Evaluation and Planning (KETEP) grant funded by the Korea government Ministry of Trade, Industry and Energy.

This work was supported by the New & Renewable Energy program (No. 2012T100100064) of the Korea Institute of Energy Technology Evaluation and Planning (KETEP) grant funded by the Korea government Ministry of Trade, Industry and Energy.

Author Contributions

Yun-Su Kim modeled and tested simulations and compiled the manuscript. Il-Yop Chung collected the data and investigated early works. Seung-II Moon supervised this work.

Appendix

A1. Derivation of Matrix A

From Equations (1)–(4), (7) and (8), a derivative of ω_e can be given as:

$$\begin{aligned} \frac{d\omega_e}{dt} &= \frac{N_{pp}}{J_{eq}}(T_e - T_m) = \frac{N_{pp}}{J_{eq}} \left[\frac{3}{2} N_{pp} i_{mq} \{ \lambda_{pm} + (L_d - L_q) i_{md} \} - \frac{-P}{\omega_m} \right] \\ &= \frac{N_{pp}^2}{2J_{eq}} [3i_{mq} \{ \lambda_{pm} + (L_d - L_q) i_{md} \} + \frac{\rho\pi r^2 v_w^3}{\omega_e} \times (\frac{110.23 N_{pp} N_{gr} v_w}{r\omega_e} - 9.30531) \\ &\quad \times \exp(\frac{-18.4 N_{pp} N_{gr} v_w}{r\omega_e} - 0.0552)] \end{aligned} \tag{23}$$

A linearization of Equation (23) around steady-state values gives:

$$\frac{d\Delta\omega_e}{dt} = a_{1,1}\Delta\omega_e + a_{1,2}\Delta i_{md} + a_{1,3}\Delta i_{mq} \tag{24}$$

From Equations (9) and (11), derivatives of i_{md} and i_{mq} can be calculated. The derivative of i_{md} can be given as:

$$\frac{di_{md}}{dt} = \frac{1}{L_d} \{ (0 - i_{md})K_{p1} + \varphi_1 K_{i1} - R_s i_{md} \} \tag{25}$$

A linearization of Equation (25) around steady-state values gives:

$$\frac{d\Delta i_{md}}{dt} = a_{2,2}\Delta i_{md} + a_{2,7}\Delta\varphi_1 \tag{26}$$

And the derivative of i_{mq} can be given as:

$$\frac{di_{mq}}{dt} = \frac{1}{L_q} [\{ (\frac{3}{2} v_{sd} i_{gd} - \frac{K_{opt} \omega_e^3}{N_{pp}^3 N_{gr}^3}) K_{p2} + \varphi_2 K_{i2} - i_{mq} \} K_{p3} + \varphi_3 K_{i3} - R_s i_{mq}] \tag{27}$$

In Equation (27), the variable v_{sd} , which is not defined as the state variable, is contained so a linearization of v_{sd} should be expressed as terms of linearization of state variables. From Equation (17), the infinite bus voltage can be given as

$$|v_{idq}| \cos \delta + j |v_{idq}| \sin \delta = v_{sd} + i_{gd} x_{TL} - j i_{gd} x_{TL} \tag{28}$$

From Equation (28), square of the magnitude of the infinite bus voltage can be given as:

$$|v_{idq}|^2 = (v_{sd} + i_{gd} x_{TL})^2 + (i_{gd} x_{TL})^2 \tag{29}$$

Since $|v_{idq}|$ is a constant value, a linearization of Equation (29) gives

$$\Delta v_{sd} = \frac{-i_{gd0} x_{TL}^2}{v_{sd0} + i_{gd0} x_{TL}} \Delta i_{gd} - x_{TL} \Delta i_{gd} \tag{30}$$

which is expressed in terms of the state variables i_{gd} and i_{gq} . By using Equation (30), Equation (27) can be linearized as:

$$\frac{d\Delta i_{mq}}{dt} = a_{3,1}\Delta\omega_e + a_{3,3}\Delta i_{mq} + a_{3,5}\Delta i_{gd} + a_{3,6}\Delta i_{gq} + a_{3,8}\Delta\varphi_2 + a_{3,9}\Delta\varphi_3 \tag{31}$$

From Equations (11) and (13), a derivative of V_{dc} can be given as:

$$\frac{dV_{dc}}{dt} = \frac{-3}{2C_{dc} V_{dc}} (v_{md} i_{md} + v_{mq} i_{mq} + v_{sd} i_{gd}) \tag{32}$$

Equation (32) contains variables v_{md} and v_{mq} that are not defined as the state variables so they should be expressed in terms of the state variables when linearizing. From Equations (9) and (11), v_{md} and v_{mq} can be linearized as:

$$\begin{aligned} \Delta v_{md} &= -K_{p1}\Delta i_{md} + K_{i1}\Delta\varphi_1 - L_q i_{mq0}\Delta\omega_e - L_q\omega_{e0}\Delta i_{mq} \\ \Delta v_{mq} &= -K_{p3}\Delta i_{mq} + \left(\frac{3K_{opt}\omega_{e0}^2 K_{p2} K_{p3}}{N_{pp}^3 N_{gr}^3} + L_d i_{md0} + \lambda_{pm}\right)\Delta\omega_e + K_{i2} K_{p3}\Delta\varphi_2 \\ &\quad + K_{i3}\Delta\varphi_3 - \frac{3K_{p2} K_{p3} i_{gd0} x_{TL}}{2}\Delta i_{gq} + L_d\omega_{e0}\Delta i_{md} + \frac{3K_{p2} K_{p3}}{2}\left(v_{sd0} - \frac{i_{gd0}^2 x_{TL}^2}{v_{sd0} + i_{gq0} x_{TL}}\right)\Delta i_{gd} \end{aligned} \tag{33}$$

By using Equation (33), Equation (32) can be linearized as:

$$\frac{d\Delta V_{dc}}{dt} = a_{4,1}\Delta\omega_e + a_{4,2}\Delta i_{md} + a_{4,3}\Delta i_{mq} + a_{4,4}\Delta V_{dc} + a_{4,5}\Delta i_{gd} + a_{4,6}\Delta i_{gq} + a_{4,7}\Delta\varphi_1 + a_{4,8}\Delta\varphi_2 + a_{4,9}\Delta\varphi_3 \tag{34}$$

Derivatives of i_{gd} and i_{gq} can be obtained from Equation (15). The derivative of i_{gd} can be given as:

$$\frac{di_{gd}}{dt} = \frac{1}{L_f} [\{(V_{dc} - 5400)K_{p4} + \varphi_4 K_{i4} - i_{gd}\}K_{p5} + \varphi_5 K_{i5} - R_f i_{gd}] \tag{35}$$

Subsequently, Equation (35) can be linearized as:

$$\frac{d\Delta i_{gd}}{dt} = a_{5,4}\Delta V_{dc} + a_{5,5}\Delta i_{gd} + a_{5,10}\Delta\varphi_4 + a_{5,11}\Delta\varphi_5 \tag{36}$$

And the derivative of i_{gq} can be given as:

$$\frac{di_{gq}}{dt} = \frac{1}{L_f} [\left\{-\frac{3}{2}v_{sd}i_{gq} - 0\right\}K_{p6} + \varphi_6 K_{i6} - i_{gq}\}K_{p7} + \varphi_7 K_{i7} - R_f i_{gq}] \tag{37}$$

Then a linearization of Equation (37) can be given as

$$\frac{d\Delta i_{gq}}{dt} = a_{6,5}\Delta i_{gd} + a_{6,6}\Delta i_{gq} + a_{6,12}\Delta\varphi_6 + a_{6,13}\Delta\varphi_7 \tag{38}$$

Derivatives of $\varphi_1 - \varphi_3$ are given in Equation (11) and by using Equations (11) and (30), their linearization can be given as

$$\frac{d\Delta\varphi_1}{dt} = a_{7,2}\Delta i_{md} \tag{39}$$

$$\frac{d\Delta\varphi_2}{dt} = a_{8,1}\Delta\omega_e + a_{8,5}\Delta i_{gd} + a_{8,6}\Delta i_{gq} \tag{40}$$

$$\frac{d\Delta\varphi_3}{dt} = a_{9,1}\Delta\omega_e + a_{9,3}\Delta i_{mq} + a_{9,5}\Delta i_{gd} + a_{9,6}\Delta i_{gq} + a_{9,8}\Delta\varphi_2 \tag{41}$$

Derivatives of $\varphi_4 - \varphi_7$ are given in Equation (15) and by using Equations (15) and (30), their linearization can be given as:

$$\frac{d\Delta\varphi_4}{dt} = a_{10,4}\Delta V_{dc} \tag{42}$$

$$\frac{d\Delta\varphi_5}{dt} = a_{11,4}\Delta V_{dc} + a_{11,5}\Delta i_{gd} + a_{11,10}\Delta\varphi_4 \quad (43)$$

$$\frac{d\Delta\varphi_6}{dt} = a_{12,5}\Delta i_{gd} + a_{12,6}\Delta i_{gq} \quad (44)$$

$$\frac{d\Delta\varphi_7}{dt} = a_{13,5}\Delta i_{gd} + a_{13,6}\Delta i_{gq} + a_{13,12}\Delta\varphi_6 \quad (45)$$

A2. Parameters of the PMSG WT System

$\rho = 1.225$ (kg/m³); $r = 83.5$ (m); $C_{dc} = 8$ (mF); $C_{p,max} = 0.4412$; $\lambda_{opt} = 7.2064$; $N_{gr} = 30$; $N_{pp} = 9$; $R_s = 8.67$ (m Ω); $L_d = 2.86$ (mH); $L_q = 3.44$ (mH); $\lambda_{pm} = 7.15$ (V·s); $L_f = 1.8$ (mH); $R_f = 0.65$ (m Ω); $x_T = 0.2371$ (Ω); $x_L = 0.0013$ (Ω).

Conflicts of Interest

The authors declare no conflict of interest.

References

1. Thresher, R.; Robinson, M.; Veers, P. To capture the wind. *IEEE Power Energy Mag.* **2007**, *5*, 34–46.
2. Goudarzi, N.; Zhu, W.D. A review on the development of wind turbine generators across the world. *Int. J. Dynam. Control.* **2013**, *1*, 192–202.
3. Global Wind Energy Council. *Global Wind Energy Outlook 2012*; Global Wind Energy Council: Brussels, Belgium, 2012. Available online: http://www.gwec.net/wp-content/uploads/2012/11/GWEO_2012_lowRes.pdf (accessed on 5 June 2013).
4. Kim, Y.-S.; Chung, I.-Y.; Moon, S.-I. An analysis of variable-speed wind turbine power-control methods with fluctuating wind speed. *Energies.* **2013**, *6*, 3323–3338.
5. Iglesias, R.L.; Arantegui, R.L.; Alonso, M.A. Power electronics evolution in wind turbines—A market-based analysis. *Renew. Sustain. Energy Rev.* **2011**, *15*, 4982–4993.
6. Benelghali, S.; Benbouzid, M.E.H.; Charpentier, J.F. Comparison of PMSG and DFIG for Marine Current Turbine Applications. In *Electrical Machines (ICEM)*; IEEE: Rome, Italy, 2010; pp. 1–6.
7. Knospe, C. PID control. *IEEE Control Systems Mag.* **2006**, *26*, 30–31.
8. Åström, K.J.; Panagopoulos, H.; Hägglund, T. Design of PI controllers based on non-convex optimization. *Automatica* **1998**, *34*, 585–601.
9. Wu, F.; Zhang, X.-P.; Godfrey, K.; Ju, P. Small signal stability analysis and optimal control of a wind turbine with doubly fed induction generator. *IET Gener. Transm. Distrib.* **2007**, *1*, 751–760.
10. Huang, H.; Mao, C.; Lu, J.; Wang, D. Small-signal modelling and analysis of wind turbine with direct driven permanent magnet synchronous generator connected to power grid. *IET Renew. Power Gener.* **2012**, *6*, 48–58.
11. Hasanien, H.M.; Muyeen, S.M. Design optimization of controller parameters used in variable speed wind energy conversion system by genetic algorithms. *IEEE Trans. Sustain. Energy* **2012**, *2*, 200–208.

12. Geng, H.; Xu, D. Stability analysis and improvements for variable-speed multipole permanent magnet synchronous generator-based wind energy conversion system. *IEEE Trans. Sustain. Energy* **2011**, *2*, 459–467.
13. Wu, F.; Zhang, X.-P.; Ju, P. Small signal stability analysis and control of the wind turbine with the direct-drive permanent magnet generator integrated to the grid. *Electr. Power Syst. Res.* **2009**, *79*, 1661–1667.
14. Mishra, Y.; Mishra, S.; Li, F.; Dong, Z.Y.; Bansal, R.C. Small-signal stability analysis of a DFIG-based wind power system under different modes of operation. *IEEE Trans. Energy Convs.* **2009**, *24*, 972–982.
15. Yang, L.; Yang, G.Y.; Xu, Z.; Dong, Z.Y.; Wong, K.P.; Ma, X. Optimal controller design of a doubly-fed induction generator wind turbine system for small signal stability enhancement. *IET Gener. Transm. Distrib.* **2010**, *4*, 579–597.
16. Valle, Y.; Venayagamoorthy, G.K.; Mohagheghi, S.; Hernandez, J.-C.; Harley, R.G. Particle swarm optimization: Basic concepts, variants and applications in power systems. *IEEE Trans. Evol. Comput.* **2008**, *12*, 171–195.
17. Ackermann, T. *Wind Power in Power Systems*; John Wiley & Sons: Hoboken, NJ, USA, 2005.
18. Lanzafame, R.; Messina, M. Horizontal axis wind turbine working at maximum power coefficient continuously. *Renew. Energy* **2010**, *35*, 301–306.
19. Abdullah, M.A.; Yatim, A.H.M.; Tan, C.W.; Saidur, R. A review of maximum power point tracking algorithms for wind energy systems. *Renew. Sustain. Energy Rev.* **2012**, *16*, 3220–3227.
20. Yazdani, A.; Iravani, R. *Voltage-Sourced Converters in Power Systems*; John Wiley & Sons: Hoboken, NJ, USA, 2010.
21. Novotny, D.W.; Lipo, T.A. *Vector Control and Dynamics of AC Drives*; Oxford University Press: Oxford, UK, 1996.
22. Leonhard, W. *Control of Electrical Drives*; Springer-Verlag: New York, NY, USA, 2001.
23. Yazdani, A.; Iravani, R. A neutral-point clamped converter system for direct-drive variable-speed wind power unit. *IEEE Trans. Energy Convs.* **2006**, *21*, 596–607.
24. Nise, N.S. *Control Systems Engineering*; John Wiley & Sons: Hoboken, NJ, USA, 2008.
25. Chung, I.-Y.; Liu, W.; Cartes, D.A.; Collins, E.G.; Moon, S.-I. Control methods of inverter-interfaced distributed generators in a microgrid system. *IEEE Trans. Ind. Appl.* **2010**, *46*, 1078–1088.
26. Eberhart, R.; Shi, Y.; Kennedy, J. *Swarm Intelligence*; Morgan Kaufmann: San Francisco, CA, USA, 2001.
27. Ozcan, E.; Mohan, C. Particle swarm optimization: Surfing the waves. *Proc. IEEE Congr. Evol. Comput.* **1999**, *3*, 1939–1944.
28. Verghese, G.C.; Perez-Arriaga, I.J.; Schweppe, F.C. Selective modal analysis with application to electric power systems, Part I: Heuristic introduction. *IEEE Trans. Power App. Syst.* **1982**, *PAS-101*, 3117–3125.
29. Kundur, P. *Power System Stability and Control*; McGraw-Hill: New York, NY, USA, 1994.